AIAA 2003-0593

Transonic Unsteady Aerodynamics of the F/A-18E at Conditions Promoting Abrupt Wing Stall (Invited)

David M. Schuster
NASA Langley Research Center
Hampton, VA

James E. Byrd
Lockheed Martin Engineering and Sciences
Hampton, VA

41st Aerospace Sciences Meeting and Exhibit
6 – 9 January 2003
Reno, Nevada

AIAA-2003-0593

Transonic Unsteady Aerodynamics of the F/A-18E at Conditions Promoting Abrupt Wing Stall

David M. Schuster*
NASA Langley Research Center, Hampton, VA 23681-2199

James E. Byrd†
Lockheed Martin Engineering and Sciences, Hampton, VA 23681-2199

Abstract

A transonic wind tunnel test of an 8% F/A-18E model was conducted in the NASA Langley Research Center (LaRC) 16-Foot Transonic Tunnel (16-Ft TT) to investigate the Abrupt Wing Stall (AWS) characteristics of this aircraft. During this test, both steady and unsteady measurements of balance loads, wing surface pressures, wing root bending moments, and outer wing accelerations were performed. The test was conducted with a wide range of model configurations and test conditions in an attempt to reproduce behavior indicative of the AWS phenomenon experienced on full-scale aircraft during flight tests. This paper focuses on the analysis of the unsteady data acquired during this test. Though the test apparatus was designed to be effectively rigid, model motions due to sting and balance flexibility were observed during the testing, particularly when the model was operating in the AWS flight regime. Correlation between observed aerodynamic frequencies and model structural frequencies are analyzed and presented. Significant shock motion and separated flow is observed as the aircraft pitches through the AWS region. A shock tracking strategy has been formulated to observe this phenomenon. Using this technique, the range of shock motion is readily determined as the aircraft encounters AWS conditions. Spectral analysis of the shock motion shows the frequencies at which the shock oscillates in the AWS region, and probability density function analysis of the shock location shows the propensity of the shock to take on a bi-stable and even tri-stable character in the AWS flight regime.

INTRODUCTION

In the mid 1990's, F/A-18E/F aircraft undergoing preproduction flight-testing encountered a lateral instability, characterized as wing drop, when performing some high-speed, high load-factor turning maneuvers[1]. This instability was ultimately traced to an Abrupt Wing Stall (AWS) of either the left or right wing causing a sudden and severe roll-off in the direction of the stalled panel. An important distinction between wing drop and AWS is that wing drop is the dynamic response of an aircraft to an aerodynamic event, while AWS is an aerodynamic event that can trigger a wing drop.

Further magnifying the importance of this aerodynamic phenomenon is the fact that a large number of jet-age fighter aircraft have encountered wing rock and/or wing drop instabilities[2]. Unfortunately, these lateral problems were not adequately predicted by developmental ground-based testing before actual aircraft flight tests. In some cases, modifying the geometry of the aircraft, such as rescheduling leading- or trailing-edge flap deflections, or adjusting flight control laws, could mitigate these instabilities. In other cases, the aircraft's operational envelope was such that the adverse behavior was rarely encountered in operational service and deemed acceptable. Unfortunately, in the case of the pre-production versions of the F/A-18E/F, the motions were relatively severe. Increases in the flight control law gains were effective in reducing the severity of the

*Senior Research Engineer, Associate Fellow AIAA.
†Staff Aeronautical Engineer.

problem, but could not completely eliminate the wing drop. Since the instability appeared in a critical portion of the flight envelope, modification of operational parameters was infeasible.

After significant expenditure of flight test and analysis resources, the lateral activity was mitigated by two modifications. First, the wing leading-edge flap deflection with Mach and angle of attack was increased, resulting in an "80% solution"[1]. However, even with the revised flap schedule the aircraft exhibited undesirable lateral activity. The second critical modification involved replacing the solid-door wing fold fairing with a porous door. Together, these modifications ultimately solved the wing drop problem on the F/A-18E/F. Though these flight-derived fixes for the F/A-18E/F solved its handling problems, the fact remains that this instability was not predicted or anticipated prior to flight test. Given the susceptibility of modern fighter aircraft to encounter uncontrolled lateral dynamics and the near-catastrophic technical and political consequences of this type of instability on the future of the F/A-18E/F program, a cooperative NASA/Navy/Air Force research effort to investigate, understand, predict, and avoid AWS on future aircraft programs has been devised and executed[3].

A key component of this research is the development of an experimental program to investigate the AWS phenomenon and devise a strategy for future testing of aircraft susceptible to AWS. One of the experimental strategies employed in this investigation focused on implementing and enhancing standard static wind tunnel test techniques that might be applied during routine aircraft development. Since AWS and the resulting lateral instabilities are dynamic or, at best highly sensitive quasi-static phenomena, measurement of unsteady wing surface pressures, loads, and accelerations were incorporated into the test procedures to investigate potential unsteady causes and/or indicators of AWS.

This paper describes the wind tunnel model employed, unsteady instrumentation, associated data acquisition techniques, summary analysis results, and their implications in the prediction and detection of the AWS phenomenon. In addition, the structural characteristics of the experimental setup were assessed and compared with the aerodynamic loads to determine if the structural flexibility of the experimental hardware was a significant contributor to the observed unsteady aerodynamics.

WIND TUNNEL MODEL, INSTRUMENTATION LAYOUT, AND DATA ACQUISITION

The model tested in the LaRC 16-Foot Transonic Tunnel (16-Ft TT) is a stainless steel 8% model of the F/A-18E. The model is the primary aerodynamic performance article used in the development of this aircraft. Since the objectives of this test involved a significant enhancement of the basic instrumentation package present on the baseline model, new wings were fabricated containing a combination of steady pressure ports, in-situ unsteady pressure transducers, outer wing accelerometers, and wing root bending strain gages. A six-component internal balance rounds out the primary instrumentation package for the model. A photograph of the model installed in the 16-Ft TT is shown in Figure 1, and a more comprehensive description of the model and test procedures is available in Reference 4.

Figure 1. F/A-18E model installed in LaRC 16-Foot Transonic Tunnel.

Several variations of the wing leading and trailing edge flap deflection were tested and evaluated. In the F/A-18E/F development program, the "80% solution" utilized the 6.1.3 version of the flight control laws and was represented during wind tunnel testing with a $10^{\circ}/10^{\circ}/5^{\circ}$ flap set, where the deflections correspond to the leading-edge flap deflection, the trailing-edge flap deflection, and the aileron deflection, respectively. In this paper, this $10^{\circ}/10^{\circ}/5^{\circ}$ wing flap set on the baseline aircraft will be highlighted. The porous-door fix implemented for the production aircraft is not included in the test data presented here. Testing was performed at atmospheric conditions over a range of Mach numbers, but the bulk of testing occurred at Mach 0.8 and 0.9. Data at Mach 0.9 are the focus of this paper.

This Mach number and flap setting are representative of conditions at which wing drop was experienced during flight test. At this Mach number, AWS is observed at angles of attack between 9° and 10°, and hereafter this will be referred to as the AWS angle of attack regime or range.

Identical steady pressure instrumentation sets were included on both the left and right wing, but due to limitations of the dynamic data acquisition and the cost and complexity of including unsteady pressure instrumentation in a model of this type, only the left wing included unsteady pressure measurements. The layout of the instrumentation package on the upper surface of this wing panel is shown in Figure 2.

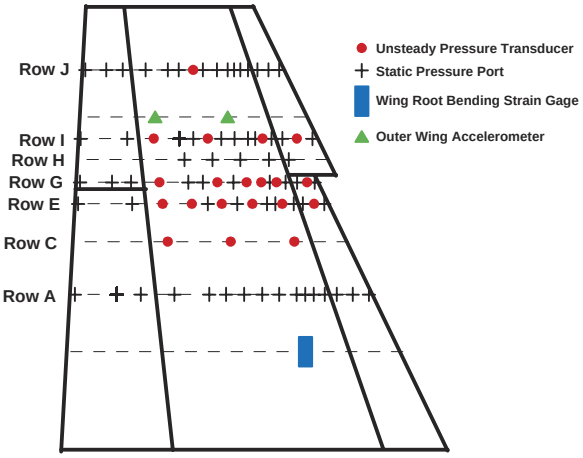

Figure 2. Instrumentation layout for the left wing upper surface.

In all, the model instrumentation consisted of 23 unsteady pressure transducers, four outer wing accelerometers, and two wing bending strain gages on which time synchronized data were acquired. Of the 23 unsteady pressure transducers, 20 were located on the upper surface of the left wing. The remaining three transducers were located on the lower surface of the left wing. Both the left and right wing were instrumented with outer wing accelerometers (two each) and wing root bending gages (one each). The dynamic data acquisition system employed in this test was capable of acquiring time-synchronized data on 32 channels; so three balance channels were also dynamically sampled. The three balance channels chosen for dynamic sampling were the axial force, pitching moment, and rolling moment components.

During the test, the unsteady data were acquired in 10-second records on magnetic tape using VHS videocassettes and digitized post-test. In the digitizing process the data were sampled at a rate of 1000 samples per second for 10 seconds. A 200 Hz anti-aliasing filter was applied to data during the digitization process. Time history records, mean, standard deviation, and maximum and minimum values were processed for each data point and channel in the dataset. The data were stored on a set of compact disks for further data processing by the AWS team.

DYNAMIC DATA ANALYSIS

In addition to simply trying to gain a physical understanding of the unsteady flow on the aircraft at AWS conditions, the analysis of the dynamic data was driven by a number of factors including wind tunnel model vibration. At test conditions where AWS had been encountered in flight, the model became quite active on the balance/sting support system exhibiting noticeable pitch, plunge, and roll vibrations. Similar balance/sting dynamics, though at somewhat higher angles of attack, are described by Mabey, et al[5]. In addition, dynamic loads monitored by the Balance Dynamics Display Unit (BDDU) indicated that the model was experiencing high axial force loads that were near and occasionally in excess of the prescribed balance limits. On several occasions, balance fouling was detected due to these oscillations. Therefore, a primary objective of the unsteady data analysis was to determine if the structural vibrations observed in the tunnel were simply a response to the extreme unsteady aerodynamics experienced at the AWS conditions, or if there was indeed an aeroelastic coupling whereby the structural oscillations had a significant, discernible impact on the unsteady aerodynamics.

To aid in this portion of the analysis, structural dynamics properties of the model, balance, and sting mounted in the 16-Ft TT were measured through simple “rap” tests of the model between test runs and a more detailed Ground Vibration Test (GVT) of the model post-test. The “rap” tests were conducted by simply hitting the model with a closed fist on the nose and wing tip of the aircraft and recording vibration time history data using the balance channels, outer wing accelerometers, and the wing root bending strain gages. A signal analyzer was used to process this time history data and produce frequency responses. Sample results of two of these tests are shown in Figure 3.

In Figure 3, several frequency peaks are labeled which correspond to dominant structural modes of the model/balance/sting system. The peak observed at 60 Hz is due to electrical interference. Hitting the forward fuselage tends to excite longitudinal structural modes such as sting and balance pitch, while hitting the wing tip excites lateral structural modes such as roll and antisymmetric wing bending. Using visual observation and experience, structural modes such as sting pitch, balance pitch, and balance roll could be matched up with observed frequencies.

The post-test GVT corroborated these results by quantitatively matching the frequencies observed in the "rap" tests to the structural motions. Results from this GVT are presented in Table 1. Of the modes listed in this table, sting vertical, balance pitch, balance roll, and antisymmetric wing bending modes were most often observed on the wing accelerometers and strain gages during periods of high model excitation in the AWS flight regime.

Unsteady readings from the balance, accelerometers, and strain gages were dominated by the structural frequencies of vibration, and independent unsteady aerodynamic traits were difficult to separate from the measurements on these instruments. Thus, the unsteady pressure measurements became the primary source of information concerning the unsteady aerodynamics present on the vehicle in the AWS flight regime.

Several methods were employed to analyze and reduce the unsteady pressure data ranging from investigation of the raw pressure time histories on individual transducers to the identification and tracking of flow structures such as shock waves.

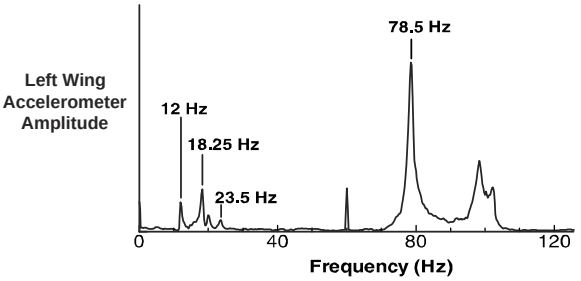

(a) Right Wing Tip Rap

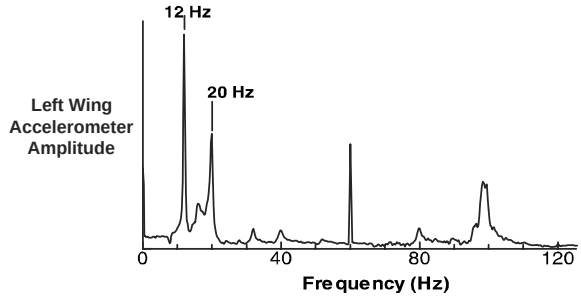

(b) Forward Fuselage Rap

Figure 3. Frequency response of a left wing accelerometer to right wing and forward fuselage raps.

Table 1. Modes and associated frequencies obtained from post-test GVT.

MODE	*FREQUENCY (Hz)*
Sting Yaw	6.86
Sting Vertical	11.69
Coupled Sting/Balance Yaw	13.06
Balance Yaw	18.71
Balance Pitch	20.21
Balance Roll	22.77
Antisymmetric Wing Bending	77.3
Balance Axial	97.8

Pressure distributions acquired on the baseline F/A-18E with $10^{\circ}/10^{\circ}/5^{\circ}$ flap set at Mach 0.9 are used in the following unsteady pressure data analyses. Pressures along Row E of Figure 2 are the primary focus of this analysis because this is the row most highly populated with unsteady transducers. It is also in close proximity to the leading edge snag, which has been identified as a key region of interest in the investigation of AWS on the F/A-18E/F[4, 6, 7].

Figure 4 shows pressure coefficient time history data acquired at a single pressure transducer on Row E near the center of the wing box at Mach 0.9. The location of this transducer is circled on the image of the planform at the bottom of the figure. Time histories are plotted in one-degree angle of attack increments from 6.5° to 9.5°. The pressure coefficient plotted in this figure is the complete pressure coefficient, as opposed to just the fluctuating component of the pressure. The vertical scale on all of the plots is identical and is also the same scale as used on subsequent plots.

Figure 4 clearly shows the progression of the shock wave forward on the wing as the angle of attack is increased into the AWS region. At 6.5°, the pressures measured by the transducer are very stable and constant across the time record. At 7.5°, the first hint of a shock moving onto this chordwise location is seen in the discrete spikes in the pressure time history. By 8.5°, the spikes are much more prevalent, and finally at 9.5° the time history is saturated with pressure spikes as the shock moves back and forth across the pressure transducer. Hwang and Pi[8] observed a similar unsteady pressure character in their buffet and wing rock analysis of the F-5A aircraft.

Figure 5 shows a similar pressure time history plot, but in this case the angle of attack is fixed at 9.5° and the series of plots represents the time histories for the entire chordwise row of transducers. There are several interesting features observed in this figure.

First, the difference between a separated flow unsteady pressure signature and the pressure signature generated by a shock passage can be seen by looking at the aft-most transducer and the four transducers in front of it. The flow separates just in front of the trailing edge flap, and the aft-most transducer shows the pressure signature for this type of flow. The transducers immediately forward of this location show the spiky nature of the pressures as shocks pass over the transducer. In addition, the amplitude of the pressure variation is considerably smaller for the separated flow case as compared to the shock passage case. The root-mean-square (rms) value of the fluctuating pressure coefficient is approximately 0.05 on the aft most transducer while it is in the range of 0.15 – 0.20 on the four forward transducers. These fluctuating pressure levels and associated flow characteristics are consistent with those quoted by Mabey in Reference 9.

The second feature to recognize in Figure 5 is that the shock is moving over the entire length of the center wing box at these conditions. Animation of the unsteady pressure distribution along this row confirms this extreme degree of shock motion. Finally, the structural vibration of the model on the sting/balance system shows up on the forward-most pressure transducer. The pressure at this location of the wing is very sensitive to angle of attack, and as the model pitches and plunges on the balance/sting support system, the pressure transducer senses the oscillation. A frequency analysis of the pressure time history on this transducer shows a peak at approximately 12 Hz, which, per Table 1, coincides with the sting vertical bending structural mode.

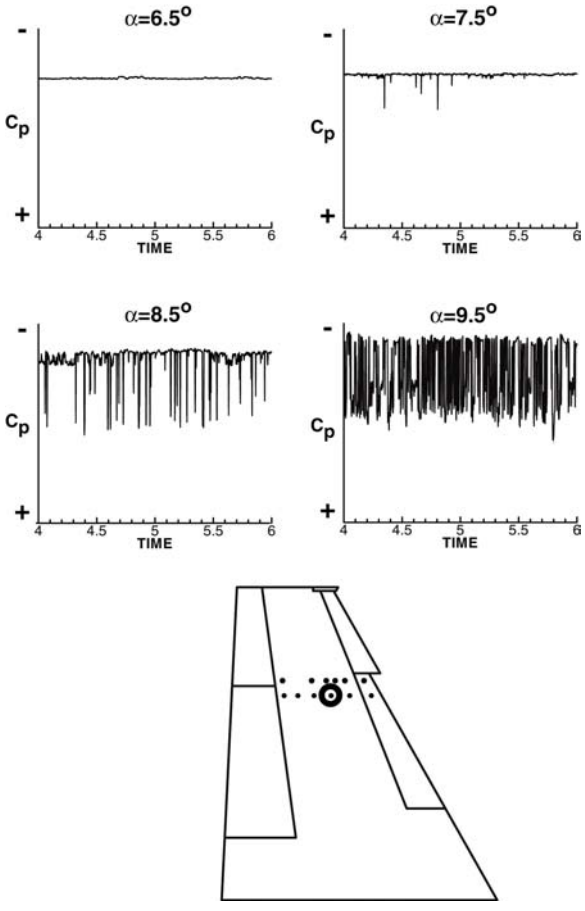

Figure 4. Pressure coefficient time history at a single point on the wing for a series of angles of attack, M = 0.90.

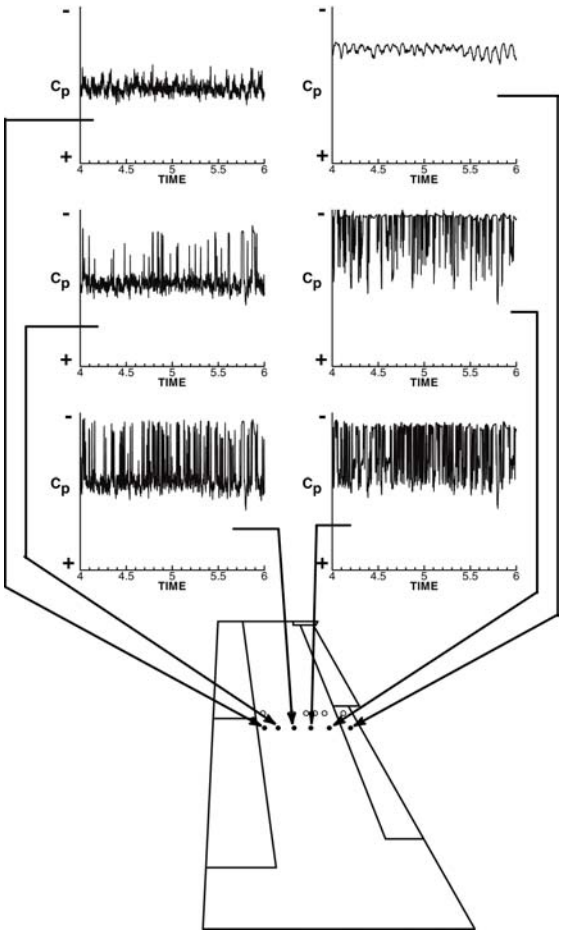

Figure 5. Pressure coefficient time histories at a constant spanwise station, M = 0.90, α = 9.5°.

Figure 6 illustrates one of the cases where a bistable character was observed in the pressure data. This figure shows the measured pressure time histories near the leading edge of the wing at 6.5°, 7.0°, and 7.5° angle of attack. At 6.5° and 7.5°, the pressure traces are stable and virtually constant, but at significantly different pressure levels. The rms value of the fluctuating pressure coefficient is on the order of 0.008 for both of these angles of attack, which, by Mabey's criteria, is typical for an attached boundary layer flow. At 7.0° the pressure tends to snap back and forth between the two pressure levels. The rms fluctuating pressure coefficient at this angle jumps to 0.11, which is indicative of a separation reattachment point. In addition, in the early part of the 7.0° time history, the pressure seems to be based at the 6.5° angle of attack level and spikes down to the 7.5° level. At about 4.6 seconds, the character of the time history changes and tends to be based at the 7.5° level of pressure spiking up to the 6.5° level. To further illustrate how tightly the 7.0° fluctuations are bounded by the pressures at 6.5° and 7.5°, a fourth plot is included in the lower right corner superimposing the time histories at the three angles of attack. Preliminary analysis suggests that this is a leading edge vortex rolling up over the pressure transducer, but CFD, pressure sensitive paint, and oil flow images have not been able to confirm this assessment.

Channel statistics were compiled for each unsteady measurement acquired in the test. These statistics included the mean value and standard deviation for each time history, as well as the maximum and minimum values. The mean and standard deviation for the complete sample was computed before searching for the maximum and minimum values.

Given this information, any individual pressure that fell outside a three-standard-deviation (3σ) band about the computed mean was excluded from consideration for the maximum or minimum pressure value because it is statistically insignificant. Plotted as standard pressure coefficient versus fraction of wing chord, these statistics provide further insight into the structure and unsteadiness of the flowfield at AWS conditions.

Figure 7 plots the mean, maximum and minimum pressures as a fraction of chord for the Row E transducers at Mach 0.9 at nominal angles of attack of 4°, 7.5°, and 9.5°. In these plots, the mean pressures are a combination of data from the steady pressure ports and the unsteady pressure transducers. Mean pressure values that do not have accompanying maximum and minimum triangles represent pressures acquired on the steady ports. At 4° angle of attack a

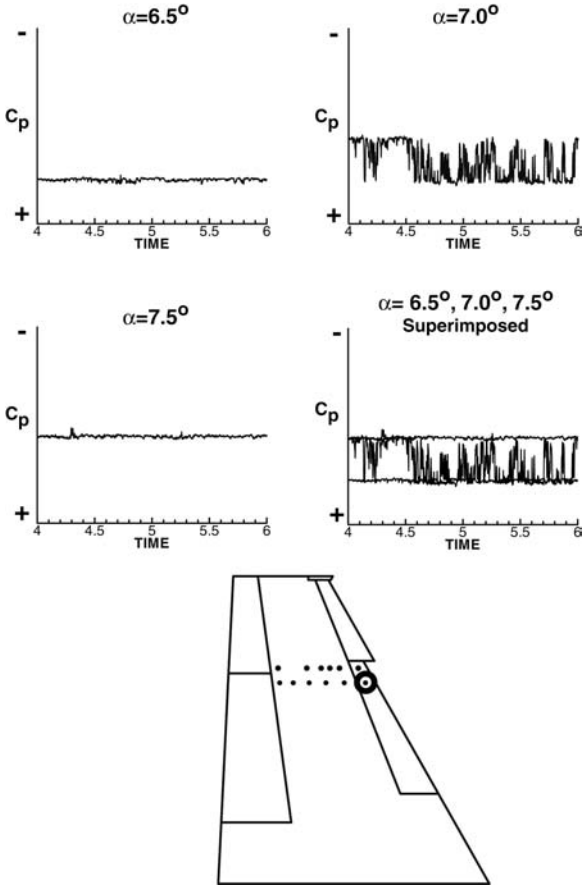

Figure 6. Pressure coefficient time histories near the wing leading edge for a series of angles of attack, M = 0.90.

shock is located on the wing in the vicinity of 65% chord, and the flow is very steady forward of the shock as evidenced by the close proximity of the maximum and minimum pressure values to their corresponding mean pressures. At 7.5° angle of attack, the mean location of the shock has moved forward to the vicinity of 40% chord and there is significant unsteadiness in the pressures in the vicinity of the shock. This angle of attack is approaching, but still well below, the AWS angle of attack range. At 9.5° angle of attack, the mean pressures show no discernible shock, but rather a smooth recompression from 16% chord to 50% chord. The unsteadiness is severe at these conditions with large differences in the maximum and minimum pressure at each measurement location between 18% and 44% chord. The smooth nature of the mean pressure in this region is misleading, and is due to the high degree of unsteadiness in the pressure distribution at this condition, which is in the heart of the AWS region for this Mach number and flap setting.

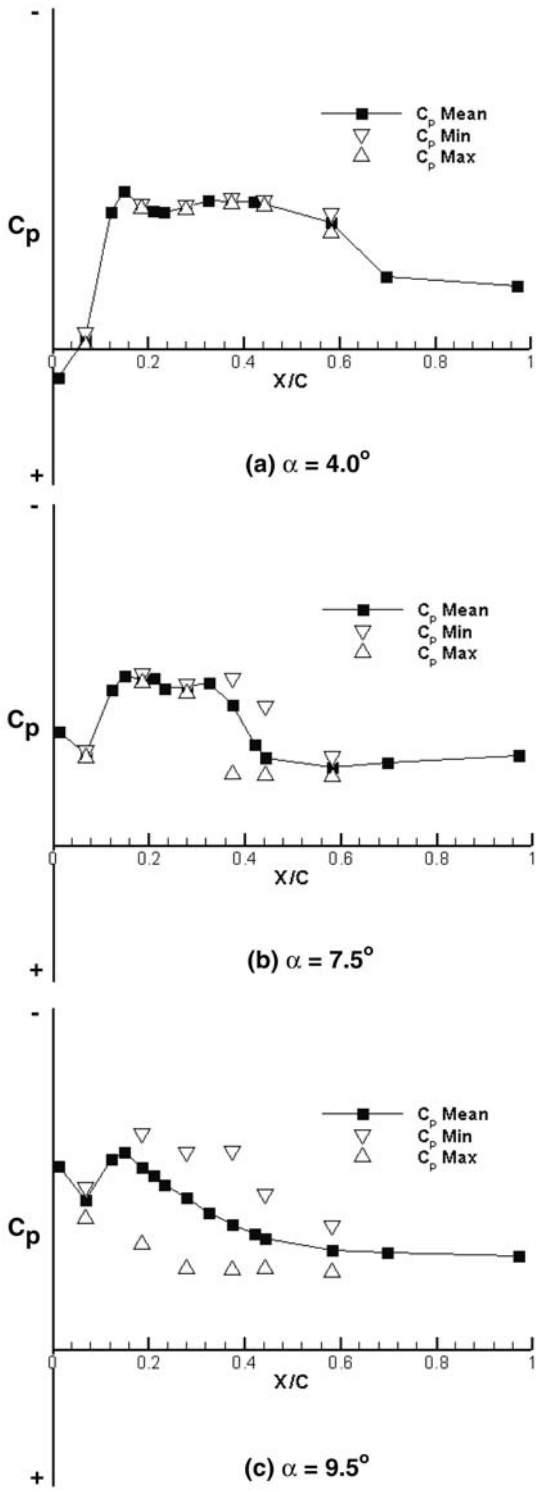

Figure 7. Row E mean, maximum, and minimum pressure distributions at three angles of attack, M=0.90.

Figure 8 further illustrates the true nature of the pressure distribution at 9.5° angle of attack. Here the instantaneous pressures at two instants in the 10-second record are superimposed on the mean, maximum and minimum pressures plotted in the previous figure. In Figure 8(a), there is a shock in the vicinity of 25% chord, while 0.4 seconds later, shown in Figure 8(b), the shock is in the vicinity of 40% chord. Animation of the instantaneous pressures clearly shows the shock moving back and forth between these two positions. However, these animations also show that the pressure distribution will momentarily stabilize in one or more configurations. Therefore, the shock motion cannot always be characterized as oscillatory and it sometimes snaps between discrete states. This behavior is an important feature of the flow, and may be a significant contributor and/or trigger for the AWS and wing drop phenomena.

In the AWS region, the shock formation and motion is a dominant feature of the unsteady flowfield. At angles of attack below the AWS region there is minimal unsteadiness in the flow. At angles of attack above the AWS region, the flow is massively separated, and while unsteady, the magnitude of the pressure fluctuation is significantly smaller than in the AWS region. To further quantify the nature of the shock and its motion in the AWS region, a simple shock tracking method has been developed as shown in Figure 9. For a given configuration at a given Mach number and angle of attack, a pressure representing the center of the shock is chosen, as designated by $C_{P_{Shock}}$ in the figure. At each point in the pressure time history record, the approximate shock location is determined by linearly interpolating for the location (X/C_{Shock}) where the instantaneous pressure distribution crosses the chosen pressure coefficient level. This effectively provides a time history of the shock location, which can be further processed.

This method has been used in this study to support two principal conclusions. The first is that there are unsteady motions of dominant flow features, namely shock waves, which do not correlate with the structural motion of the vehicle. In other words, the unsteady aerodynamics experienced on the F/A-18E model at AWS conditions are not a direct result of the structural vibrations encountered due to the balance/sting support system. This conclusion is borne out in Figures 10 and 11, which compare the frequency response of the shock location for the Row E pressures with the frequency response for the wing root bending strain gage. The shock location data represents the primary unsteady aerodynamic forcing

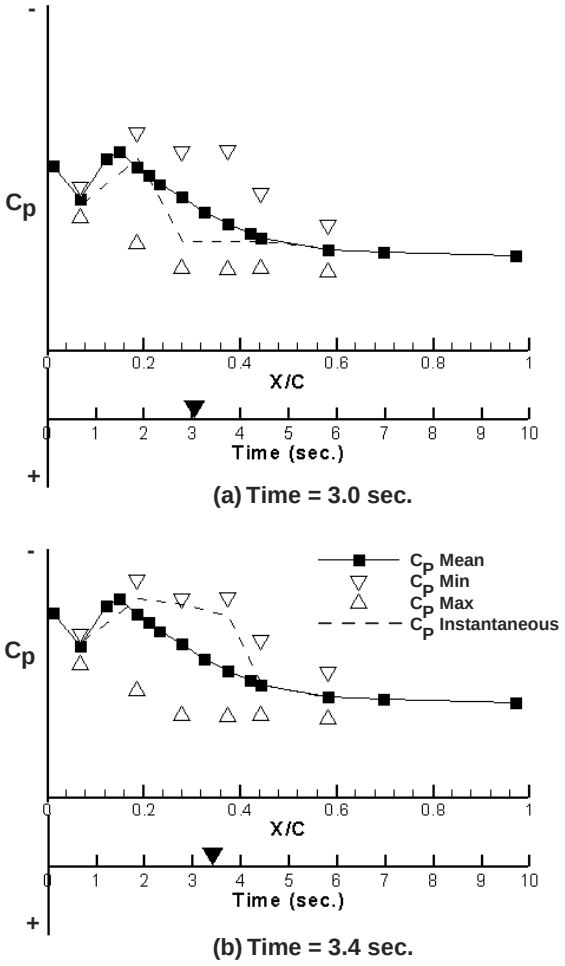

Figure 8. E-row pressure distributions including instantaneous pressures at two different times, M=0.90, α=9.5°.

function applied to the system, while the strain gage data represents the structural response of the system. Figure 10 makes the comparison at Mach 0.9 and 6.5° angle of attack, which is below the AWS angle of attack region of interest. Figure 11 makes the same comparison with the same plotting scale factors at 9.5° angle of attack, where the aircraft is in the middle of the AWS angle of attack range.

The first thing to note is the significant difference in the magnitude of structural response between the two angles of attack. At 6.5°, the strain gage data has much lower amplitude with a similar frequency content to the 9.5° angle of attack case. The frequency response of the strain gage is characterized as relatively discrete peaks at frequencies that can be correlated with those of Table 1. In contrast, the shock motion in both figures is characterized by a large number of peaks of similar amplitude over a

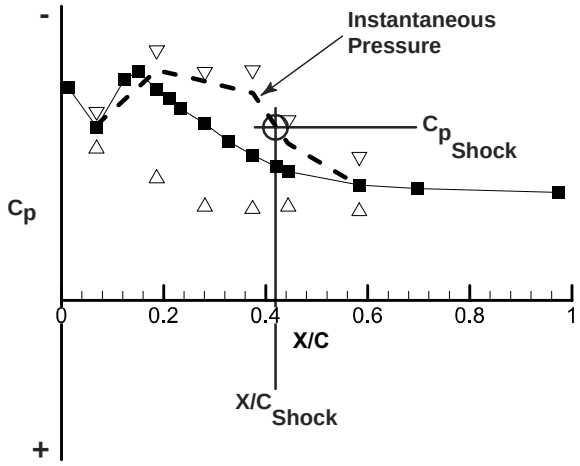

Figure 9. Strategy implemented for tracking shock motion.

relatively broad band of frequencies. More importantly, there are no particularly strong peaks in the shock motion frequency response that can be directly correlated with a structural frequency. Therefore, it is concluded that the unsteady aerodynamics, at least those represented by the shock motion, would be present on the model despite the structural vibrations encountered during wind tunnel testing. It should also be noted that given the 8% scale of the wind tunnel model, any frequency less than 25 Hz would scale to a frequency of less than 2 Hz on the full-scale aircraft. Therefore, there is a significant source of full-scale low-frequency unsteady aerodynamics generated by the shock motion that may not be effectively damped by the flight control system.

The second significant conclusion reinforced by the shock motion data is that the shock is not smoothly oscillating across the surface of the wing at a given set of aerodynamic conditions. Rather, it tends to stabilize at discrete locations, and rapidly transitions between locations. This is illustrated in Figure 12, which plots the probability of the shock being located at a specific chordwise point on the wing for four angles of attack at Mach 0.9. At 6.5° angle of attack the shock is primarily located at 41% chord, with a significantly lower probability that it would be located at 52% chord. In short, at these conditions, the shock motion is limited to approximately 11% of the local wing chord, and it is relatively stable at 41% chord. The probability of the shock being located at positions other than these two locations is small at 6.5° angle of attack. At 7.5° angle of attack, the shock motion is still confined to two locations, but these locations have moved forward on the wing, now at 33% and 41% chord and there is less preference for the shock to be located at the forward position than there was at 6.5° angle of attack. At 8.5° angle of

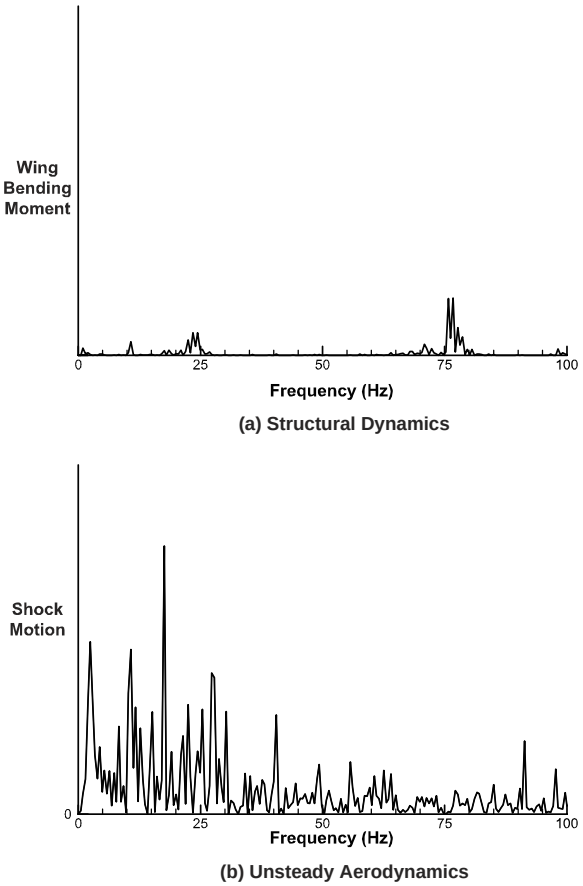

Figure 10. Comparison of model structural dynamic and unsteady aerodynamic frequency content, M=0.90, α=6.5°.

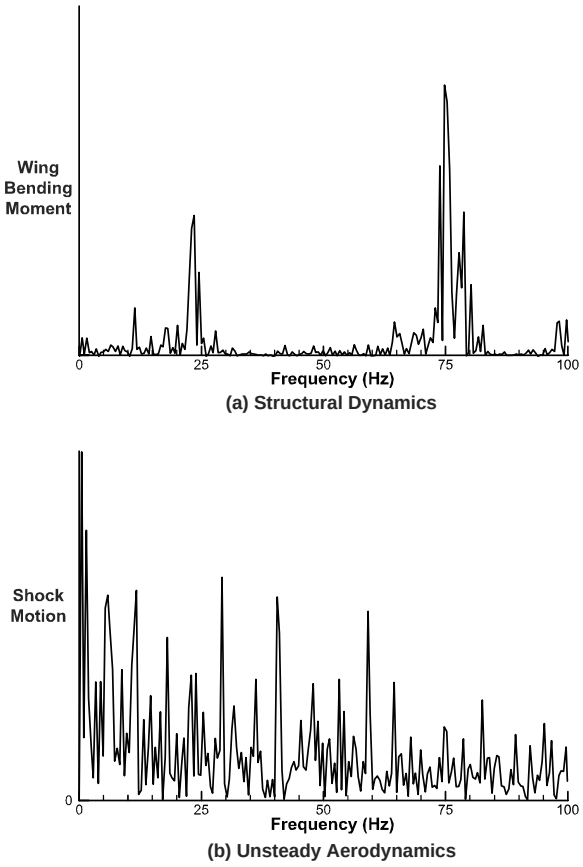

Figure 11. Comparison of model structural dynamic and unsteady aerodynamic frequency content, M=0.90, α=9.5°.

attack a third peak shows up in the probability density function forward of the two peaks identified at the previous angles of attack. The locations where the shock is most likely to be present are now at 26%, 35%, and 42% chord. It is still most likely that the shock will be located at one of the aft two locations, but at this angle of attack, the shock now regularly moves as much as 16% of the wing chord. Finally at 9.5° angle of attack there are two primary peaks where the shock resides, 28% and 37% chord, but the shock regularly travels as far back as 43% chord and as far forward as 16% chord. This gives a regularly observed range of shock motion of 27% chord at 9.5° angle of attack. The change in aerodynamic load that can be attributed to such a range of shock motion is significant, and if this shock motion were to occur asymmetrically on the left and right wings, the rolling moments could be large enough to trigger a lateral event such as wing drop. Forsythe and Woodson[10] demonstrate this type of asymmetric behavior using an unsteady Detached-Eddy Simulation (DES) of the full-span F/A-18E aircraft.

CONCLUDING REMARKS

A wind tunnel test has been conducted measuring a number of unsteady quantities on an 8% scale model of the F/A-18E at conditions where AWS has been encountered on the full-scale aircraft. Among these quantities, the unsteady pressures provide the best insight into the aerodynamic flowfield present on the aircraft at AWS conditions. Accompanying measurements, including outer wing accelerations, wing root bending moments, and load balance dynamics, were dominated by the structural dynamics of the model/balance/support system. While useful for general assessment of the unsteadiness of the aerodynamics influencing the model, they cannot be used to effectively investigate the details of the unsteady flow phenomena present on the aircraft.

The unsteady pressures have been examined both in raw data form and statistically. The raw time histories of the pressures at individual transducer locations clearly showed areas of separated flow as well as extensive shock wave motion on the wing upper surface. This is particularly true in the vicinity

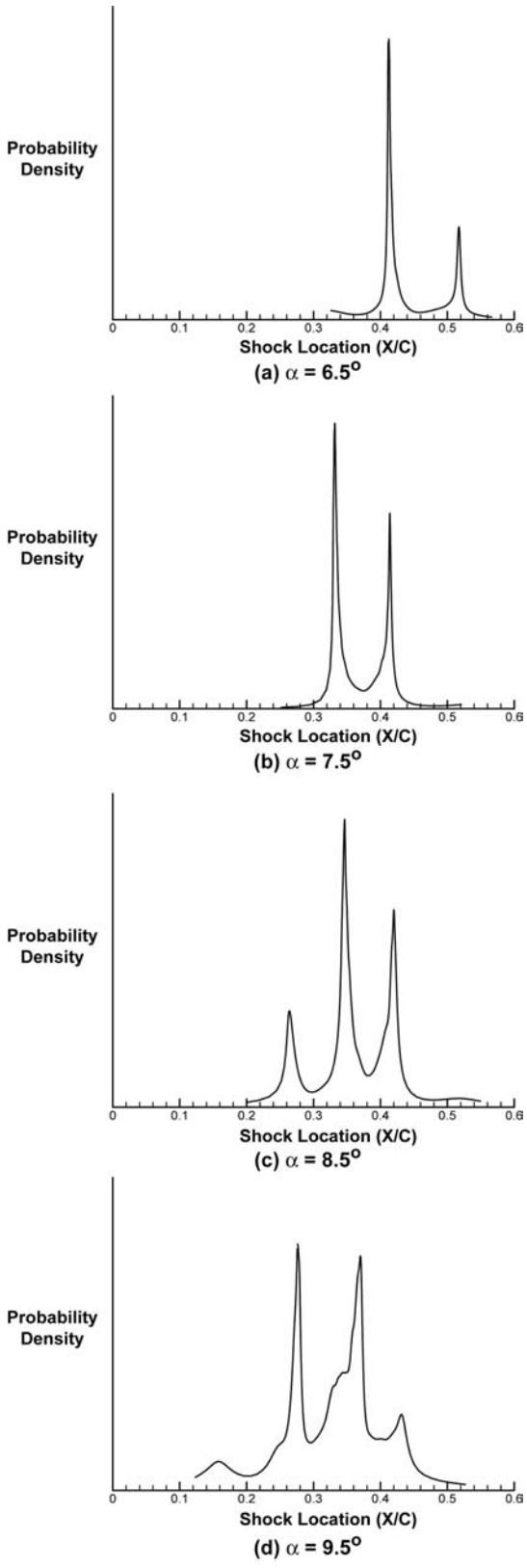

Figure 12. Probability of the Row E shock being located at a given X/C for four angles of attack, M=0.90.

of the leading edge snag on the F/A-18E, which has been identified as a primary contributor to the lateral instabilities of the aircraft.

Animations, although impossible to show in this paper, and statistical analysis of the chordwise pressure distributions further confirm the large-scale shock motion present on the wing and the angle of attack range over which this motion is present. At AWS conditions, Mach 0.9 and 9.5° angle of attack, shock motion is greatest with movement in excess of 25% of the local wing chord. Shock excursions of this magnitude typically result in large changes in wing loads. The shock motion on the model also shows significant frequency content below 25 HZ, which scales to less than 2 Hz for the full-scale aircraft. This is significant since the combination of large-scale shock motion and low frequency provide a potential triggering mechanism for lateral instabilities, such as wing drop, which probably could not be effectively damped by the automatic flight control system.

In general, the structural vibrations of the model do not heavily influence the pressures. More importantly the frequency response for the terminal shock on the wing does not correlate with the structural vibration frequencies of the model/balance/sting support system.

Finally, statistical analysis of the shock motion exhibits a bi-stable and even tri-stable character of the shock motion and location in the AWS flight regime. The shock does not tend to smoothly oscillate between chordwise locations on the upper surface of the wing, but rather it tends to linger at discrete locations, snapping back and forth among them. This characteristic certainly suggests a potential mechanism for a wing drop event where the right wing may be at one stable shock state while the left wing is at another and vice versa.

The measurement of unsteady pressures has provided a great deal of diagnostic insight into the complex flow structure present on the F/A-18E wing at AWS conditions. However, the value of unsteady measurements in screening for AWS in a routine testing environment is open for debate. The workforce and hardware resources required to acquire, reduce, and analyze unsteady pressure data are significant. Without solid techniques and procedures for incorporating unsteady pressures in an AWS screening process, the additional cost of acquiring unsteady pressure data is likely too high for most programs.

Further research is required into how unsteady pressures might be readily used to screen for AWS. A definite recommendation is that unsteady pressure transducers should be included on both wings of the

aircraft as opposed to just the single wing in this study. Lateral phenomena could be readily extracted and separated from longitudinal phenomena using time synchronized pressure data from both wings. This would likely provide an entirely new insight into the AWS phenomenon. In addition, the overall coverage of unsteady transducers should be increased over that used in the present study. This would probably require a larger scale model and it would surely require a more complex and capable dynamic data acquisition system than used in this analysis.

ACKNOWLEDGEMENTS

This work was supported by the NASA Aerospace Systems Concepts to Test (ASCoT) program, NAVAIR, and the Office of Naval Research.

REFERENCES

1. Traven, R., Hagan, J., and Niewoehner, R., "Solving Wingdrop on the F-18E/F Superhornet, 1998 Report to the Aerospace Profession, Society of Experimental Test Pilots, September 1998, pp. 67-84.
2. Chambers, J. and Hall, R., "Historical Review of Uncommanded Lateral-Directional Motions at Transonic Conditions," AIAA-2003-0590, January 2003.
3. Hall, R. and Woodson, S., "Introduction to the Abrupt Wing Stall (AWS) Program," AIAA-2003-0589.
4. McMillin, N., Hall, R., and Lamar, J., "Understanding Abrupt Wing Stall with Experimental Methods (Invited)," AIAA-2003-0591, January 2003.
5. Mabey, D. G., Welsh, B. L., and Pyne, C. R., "A Review of Rigid Body Response on Sting Supported Models at High Angles of Incidence," ***Progress in Aerospace Sciences***, Vol. 28, 1991, pp. 133-170.
6. Woodson, S. Green, B., Chung, J., Grove, D., Parikh, P., and Forsythe, J., "Understanding Abrupt Wing Stall (Invited)," AIAA-2003-0592, January 2003.
7. Parikh, P and Chung, J., "A Computational Study of the AWS Characteristics for Various Fighter Jets: Part I, F/A-18E & F-16C," AIAA-2003-0746.
8. Hwang, C. and Pi, W. S., "Investigation of Steady and Unsteady Pressures Associated with the Transonic Buffeting and Wing Rock of a One-Seventh Scale Model of the F-5A Aircraft," NASA Contractor Report 3061, 1978.
9. Mabey, D. G., "Unsteady Aerodynamics: Retrospect and Prospect," ***The Aeronautics Journal of the Royal Aeronautical Society***, Review Paper No. 003, January 1999.
10. Forsythe, J. and Woodson, S., "Unsteady CFD Calculations of Abrupt Wing Stall Using Detached-Eddy Simulation," AIAA-2003-0594, January 2003.